THE UNIVERSITY of EDINBURGH

Edinburgh Research Explorer

Modelling the influence of steel structure compartment geometry on travelling fires

General rights
Copyright for the publications made accessible via the Edinburgh Research Explorer is retained by the author(s) and / or other copyright owners and it is a condition of accessing these publications that users recognise and abide by the legal requirements associated with these rights.

Take down policy
The University of Edinburgh has made every reasonable effort to ensure that Edinburgh Research Explorer content complies with UK legislation. If you believe that the public display of this file breaches copyright please contact openaccess@ed.ac.uk providing details, and we will remove access to the work immediately and investigate your claim.

OPEN ACCESS

Download date: 22. Jan. 2021

Modelling the influence of steel structure compartment geometry on travelling fires

Author 1

- Marion Charlier, Research engineer
- ArcelorMittal Global R&D, Esch/Alzette, Luxembourg
- https://orcid.org/0000-0001-7690-1946

Author 2

- Antonio Gamba, PhD candidate
- Department of Urban and Environment Engineering (UEE), Liege University, Liège, Belgium.
- https://orcid.org/0000-0001-5937-577X

Author 3

- Xu Dai, BEng, MSc, PhD
- School of Engineering, BRE Centre for Fire Safety Engineering, The University of Edinburgh, Edinburgh, United Kingdom
- https://orcid.org/0000-0002-9617-7681

Author 4

- Stephen Welch, MA (Cantab), MSc, PhD
- School of Engineering, BRE Centre for Fire Safety Engineering, The University of Edinburgh, Edinburgh, United Kingdom
- https://orcid.org/0000-0002-9060-0223

Author 5

- Olivier Vassart, Professor
- ArcelorMittal Steligence®, Esch/Alzette, Luxembourg
- https://orcid.org/0000-0001-5272-173X

Author 6

- Jean-Marc Franssen, Professor
- Department of Urban and Environment Engineering (UEE), Liege University, Liège, Belgium.
- https://orcid.org/0000-0003-2655-5648

Full contact details of corresponding author.

Marion Charlier

Research Engineer

marion.charlier@arcelormittal.com

ArcelorMittal Global R&D, Esch/Alzette, Luxembourg

Abstract (150 – 200 words)

The response of structures exposed to fire is highly dependent on the type of fire that occurs, which is in turn very dependent on the compartment geometry. In the frame of the European RFCS TRAFIR project, CFD simulations using FDS software were carried out to analyse the influence of compartment geometry and the interaction with representative fuel loads to explore the conditions leading to the development of a travelling fire. The influence observed of ceiling height, crib spacing, and opening geometry in controlling spread rates tend to confirm the possibility to predict the occurrence, or not, of travelling fire. The results of one CFD analysis are then used to perform a nonlinear thermomechanical analysis of a steel structure with SAFIR® software. Indeed, it is possible to use the radiative intensities and gas temperatures obtained with CFD to calculate with FEM the temperatures in structural elements located in the compartment, and to evaluate the structural behaviour of a frame made of these elements. This paper therefore highlights the effect of building design specifications on the temperature development and on the resulting mechanical behaviour of a steel structure that considers comprehensively the travelling nature of the fire.

Keywords chosen from ICE Publishing list
Fire engineering
Computational mechanics
Steel structures

List of notations (examples below)

RFCS	Acronym for "Research Fund for Coal and Steel"
CFD	Computational Fluid Dynamics
FEM	Finite Element Method
$D*/\delta x$	non-dimensional parameter to assess the quality of the mesh in FDS
VENT	Used to prescribe planes adjacent to obstructions or external walls in FDS
HRRPUA	Heat Release Rate per Unit Area (kW/m^2)
CPU	Central Processing Unit

1   **Introduction**

2   Small compartment fires behave in a relatively well understood manner, usually defined as post-

3   flashover fires, where the temperatures within the compartment are considered to be uniform.

4   Yet, fires in large compartments do not always reach a post-flashover fire state and there is

5   instead a more localised fire that may travel within the compartment. More recently, the

6   "travelling fire" terminology (Stern-Gottfried and Rein, 2012; Dai et al., 2020) has been used to

7   define fires burning locally and moving across entire floor plates over a period of time. Several

8   studies (Horová et al., 2013; Rush et al., 2015; Hidalgo et al., 2017) have been presented about

9   the behaviour of a structure when it is subjected to a travelling fire. These experimental

10   campaigns provide first insights regarding the parameters influencing fire spread, such as heat

11   release rate density and wood moisture content. Furthermore, in 2005, an experimental

12   programme (Thomas et al., 2005) was set in a deep enclosure and the main conclusion was

13   that fires in deep compartments are strongly affected by the ventilation. Nevertheless, no proper

14   information or scientific knowledge has been established yet on the configurations that can lead

15   to the development of travelling fires (Dai et al., 2017). In the frame of the TRAFIR project,

16   several CFD numerical simulations were made to identify the parameters that may lead to a

17   travelling fire. This paper presents some of these simulations and explains how the CFD results

18   can be used to perform a numerical analysis of the temperature development and resulting

19   mechanical behaviour of a steel structure that considers comprehensively the travelling nature

20   of the fire.

21

22   **2. THE SETUP OF CFD SIMULATIONS AND ITS CORRESPONDING ASSUMPTIONS**

23

24   *2.1 Computational domain*

25   The Fire Dynamics Simulator (FDS, version 6.7.0) is adopted as the numerical simulation tool.

26   The cell size used in the FDS models depends highly on the situation that is modelled and on

27   the purpose of the simulation. For simulations involving buoyant plumes, the FDS User's Guide

28   (McGrattan et al., 2017) defines a non-dimensional parameter to assess the quality of the mesh:

29   $D^*/\delta x$. In all the hereafter described simulations, cell size of 0.25m x 0.25m x 0.25m was

30   considered. These values were not based on a sensitivity analysis but on existing analyses

31 representing fire dynamics in large enclosures. Indeed, the FDS Validation Guide contains a

32 table of the values of D*/δx used in the simulation of the validation experiments which were

33 used as guidance. Extra cells have been defined outside the compartment boundaries in order

34 to consider the coupling to the external environment.

35

36 ***2.2 Fire load***

37 The fire load is supposed to be made of discrete wood cribs. No detailed representation of a

38 wood crib (i.e. involving alternation of sticks and air gaps) was used but a simpler approach was

39 adopted, using 1m^3 solid cubes. This approach is based on the work done by (Degler et al.,

40 2015) and (Horová, 2015). It was also used by (Dai et al., 2019); each box was prescribed with

41 experimental measured mass loss and the experimental thermal field development was

42 successfully reconstructed. The overall heat release rate was used as input to VENTs, with

43 each VENT representing a wood crib burning surface (the VENT group is used to prescribe

44 planes adjacent to obstructions or external walls). The wood constituting the cubes is assumed

45 to be red oak type with the following chemical composition: $C_{3.4}H_{5.78}O_{2.448}N_{0.0034}$ and a soot yield

46 of 0.0015 g/g. These values are adopted from the Society of Fire Protection Engineers

47 Handbook (2002). The properties of the modelled wood are: conductivity 0.1 W/m/K, specific

48 heat 1.3 kJ/kg/K, emissivity 0.9 and density 400 kg/m^3. The predefined HRRPUA curve

49 considered come from Degler et al.: it was first obtained numerically using the complex pyrolysis

50 model in FDS then validated by comparison with pallet HRRPUA curves obtained

51 experimentally. The HRRPUA curve has a peak at 480 kW/m^2 and lasts for 33 minutes in total.

52 The Heat Release Rate curve resulting from one cube burning is depicted on Fig. 1.

53 ***2.3 Fire spread and heat release rate***

54 Planar devices were placed on each face of the cribs (except on the face in contact with the

55 floor) to measure the temperatures on the solid surfaces. In FDS, quantitative results can be

56 obtained through the use of devices, evaluated using cell centered or face centered values of

57 the cell the device is located in. Devices on solid surfaces allow prescribing a solid phase

58 quantity, and they can be coupled with a spatial statistics option (in which case the output

59 quantity is not associated with just a single point on the surface). The special statistics option

60 MAX was used, and caused FDS to write out the maximum value of the surface temperature

61   over the cells that are included in the specified bounded volume. If the surface temperature

62   reaches 300°C on at least one face of the volume, then the five surfaces are set to start burning

63   following the prescribed HRRPUA (Heat Release Rate Per Unit Area) curve. This temperature

64   of ignition was arbitrarily set equal to 300°C, which is a reasonable approximation of ignition

65   temperature for certain cellulosic materials (Society of Fire Protection Engineers Handbook,

66   2002). Before reaching ignition, the face heating is computed by FDS considering radiative and

67   convective heat transfers from the surroundings. When ignition occurs, the HRPRUA curve

68   starts as prescribed, with no further consideration of the radiative and convective exchanges

69   with the surroundings: FDS generates combustible gases that, if entirely burnt, will result in the

70   prescribed heat release rate. Nevertheless, if insufficient oxygen is available, some gas may be

71   left unburnt and the released heat will therefore be less than the one prescribed.

72

73   ***2.4 Boundary conditions***

74   The openings represented in the models are present from the beginning of the fire. Walls and

75   ceiling are made of 25 cm thick concrete (conductivity 2.4 W/m/K, specific heat 1 kJ/kg/K,

76   density 2400 kg/m^3). In all of the compartments presented in this paper, openings are present

77   on both walls along the X axis, and centred. For the sake of clarity, the X and Y axis mentioned

78   hereafter correspond, respectively, to the horizontal and the vertical axis of plan views of the

79   compartments.

80

81   ***2.5 Radiation***

82   The number of radiation angles was set to 100, i.e. the value prescribed by default in FDS. The

83   flame temperature (as opposed to the average cell temperature) is not reliably calculated in a

84   large-scale fire simulation because the flame sheet is not well-resolved on a relatively coarse

85   numerical grid (McGrattan et al., 2017). This implies that the source term in the radiation

86   transport equation cannot be reliably calculated. A practical alternative to this limitation is to

87   prescribe the radiative fraction, which specifies explicitly the fraction of the total combustion

88   energy that is released in the form of thermal radiation. The FDS default value of radiative

89   fraction, 35%, was not modified and this constitutes a basic assumption of the presented model.

90

91   **3. MODEL OF DIFFERENT CONFIGURATIONS OF LARGE COMPARTMENTS: RESULTS**

92   **AND INFLUENCES**

93   Different typologies of large compartments were modelled: the conditions supporting travelling

94   fire development are explored by varying some of the fundamental inputs to the model, i.e.

95   ceiling height, opening size, fuel load density and compartment layout. Two series of

96   configurations are investigated, in which series 1 relates to a deep rectangular compartment

97   and series 2 relates to a large square compartment. Table 1. summarizes the different

98   configurations analysed in the frame of this paper.

99

100   *Table 1.* Different configurations of large compartments

Config.	Compartment dimensions X,Y,Z (m)	CFD Domain dimensions X,Y,Z (m)	Opening size (m)	Opening factor m$^{1/2}$	Separation between the cribs (m)	Fire load (MJ/m^2)
1.a	50 x 10 x 4	60 x 12 x 6	45 x 3.5	0.40	1	550
1.b	50 x 10 x 4	60 x 12 x 6	20 x 3.25	0.16	1	550
2.a	20 x 20 x 8	24 x 24 x 9	16 x 6.75	0.39	2	270
2.b	20 x 20 x 3.5	24 x 24 x 4	16 x 2.25	0.10	2	270

101

102   ***3.1 Deep rectangular compartment – 1D spread***

103   In configuration 1, a 50m x 10m x 4m compartment is defined in a model domain of 60m x 12m

104   x 5m. The openings extend vertically from 0.25m above floor level. In both configurations (1.a

105   and 1.b) the fire starts by the ignition of the wood crib placed at the left-end of the compartment,

106   at mid-width (see Fig. 2). Figures 3,4,5 and 7 depict iso-lines representing the fire front edge

107   locations at different times. According to Fig. 3, in configuration 1.a the fire spreads slowly at the

108   beginning (0m – 15m), then faster (15m – 50m) when the effects of pre-heating by radiation

109   from the hot layer become more significant. Specifically, at beginning of the fire (0 – 20

110   minutes), the pattern of the burning area indicates a t^2 development, but the acceleration is

111   soon damped with the remaining spread being closer to a steady rate of increase along the

112   length of the compartment. Steady spread can be expected when the process is being driven

113   primarily by local crib-to-crib spread and where the effects of preheating from the hot layer to

114   cribs ahead of the front is relatively minor, and does not significantly increase with time. Also,

115   the fire spread front edge has a clear time lag when it is in the area near the openings, as

116   depicted on Fig. 3 around y=0m and y=10m. This may be due to the fact that in those areas the

117   pyrolysis is moderated by exposure to the adjacent cold ambient air and the main combustion

118   zone at the diffusion interface in the gas phase is not moving ahead of the pyrolysis zone. As

119   shown in Fig. 3 and Fig. 4, the fire spreads much faster overall under configuration 1.b

120   compared with configuration 1.a. Indeed, configuration 1.b requires 52 minutes to spread over

121   the whole compartment compared to 90 minutes for configuration 1.a. This can be explained by

122   more energy leaving the compartment through the larger openings of configuration 1.a.

123   Compared with configuration 1.a, the compartment of configuration 1.b is more likely to increase

124   the fire spread rate, due to greater retained heat but also due to the burning zone seeking

125   oxygen towards the openings (0m – 10m). For both configurations, the prescribed Heat Release

126   Rate matches the computed value obtained from the code, implying no significantly ventilation

127   controlled situations.

128

129   Some interesting differences are also apparent in the instantaneous fire spread rate evolution.

130   The speed at the horizontal centreline, versus X location, is directly represented in Fig. 5. The

131   values are determined from the straight-line distance between two ignited wood crib centres

132   (mm) divided by the time for the second wood crib being ignited (s) and for each of these

133   values, the depicted relative X location corresponds to the mid-distance between two ignited

134   wood cribs. Thus, higher velocity regions of the chart represent rapid transitions between cribs,

135   but are of relatively short duration. In configuration 1.b when the fire has passed the opening

136   (10m – 20m), more oxygen is available to sustain more vigorous combustion, and compensating

137   to some extent for the reduction in retained heat. This may be part of the reason that the fire

138   spread rate is higher in this region, compared with the region from 0m – 10m. Then the fire

139   spread rate decreases from 30m – 35m as access to oxygen diminishes towards end of

140   opening. In configuration 1.b, at the region of 35m – 50m, the fire spread rate increases again,

141   due to heat retention in the more enclosed region, though much of the gas-phase combustion

142   may still be located near the opening at around 35m. Moreover, as shown in Fig. 5, the fire

143   spread rate in configuration 1.b is at times significantly higher than the one in configuration 1.a.

144   Overall, compared to the more open configuration 1.a, the fire travel format in configuration 1.b

145   is less steady, being strongly influenced by phenomena associated with the smaller openings.

146

147   For all wood cribs of configuration 1.a, the triggered surface is the one facing the previous cribs,

148   revealing that the radiation of the previous burning wood crib might play the major role in the fire

149   spread. For configuration 1.b, it is also the case for the wood cribs situated at the left end of the

150   compartment and the right end of the openings. However, for the wood cribs at the left end of

151   the openings and at the right end of the compartment, the triggered surface is the one facing the

152   ceiling due to the radiation from the hot smoke layer. This implies that the presence of openings

153   changes the fire spread mechanism, as has been observed experimentally (Gupta et al. 2020).

154   For both configurations, the Heat Release Rate computed by FDS coincides with the imposed

155   Heat Release Rate (prescribed through HRRPUA curves), which confirms that there is no

156   unburnt gaseous fuel.

157

158   **3.2 Square compartment – 2D spread**

159   In configurations 2.a and 2.b, the compartment dimensions are respectively 20m x 20m x 8m

160   and 20m x 20m x 3.5m and the model domains respectively 21m x 21m x 9m and 24m x 24m x

161   4m. The openings are placed 0.25m above floor level. The fire starts by the ignition of the wood

162   crib placed at the centre of the compartment and the fire load consists of $1m^3$ wood cribs

163   spaced 2m away from each other. This fuel density was chosen to represent the rate of heat

164   release density of an office building prescribed by the Annex E of Eurocode 1 (EN1991-1-2,

165   2002), which is 250 kW/m^2. When compared with configurations 1, the results indicate generally

166   slower spread rates, which is consistent with the greater crib spacing. Also, a 2D spread is

167   observed in both cases, but with a slightly slower spread at the openings side for configuration

168   2.a where less heat is retained, as depicted in Fig. 6.a. In configuration 2.b the fire spread

169   accelerates more rapidly, taking 28 minutes to spread over the entire floor versus 45 minutes in

170   configuration 2.a. This difference is suggested to result mainly from lowering the ceiling height,

171   due to the stronger coupling between the hot gases and the pyrolyzing cubes. The change of

172   opening factor also impacts on the ventilation airflows at the openings, and the more regular

173   spread depicted on Fig. 6.b is a net result of the enhanced heat transfer with the lower ceiling,

174   together with changes in burning behaviour related to ventilation differences and the reduced

175   overall duration of spread.

176

4. LINKING CFD AND FEM: RESPONSE OF A STEEL STRUCTURE TO THE TRAVELLING FIRE CHARACTERISTICS

4.1 Modelling strategy

The CFD analyses are performed with a model of the compartment that does not necessarily contain the structural elements (Welch et al., 2008; Tondini et al., 2016). Structural elements must be present in the CFD model if they form a boundary of the fire compartment (walls and ceiling slab) or if they significantly influence the mass flow or the radiative flow in the compartment (deep concrete beams, wide columns, shear walls…). If the structure is made of linear steel members, it is likely that the characteristic size in the transverse direction of the steel elements is small with respect to the characteristic length of the compartment, which can justify the absence of these elements in the CFD domain. A dedicated version of FDS 6 has been written where the sole modification is the creation by FDS of a new file in which particular results are written to be used by the subsequent structural analysis by SAFIR (Franssen and Gernay, 2017). The coupled code has previously been verified in the frame of to two practical examples: a steel rack system next to a pool fire (Tondini et al., 2012) and an open car park (Tondini et al., 2016)". The results are:

- gas temperature, used for the convective heat transfer to the structural elements;
- coefficient of convection, depends on the gas velocity. NB – SAFIR does not currently use this coefficient; it uses a constant value, for example 35 W/m²K, for simplicity;
- radiation intensity in several directions. These intensities have been preferred to the impinging flux or the adiabatic surface temperature for different orientations, because these latter quantities both result from an integral on a surface and the information about the direction of the impinging intensities considered in these integrals is lost, with the consequence that concave sections cannot be considered appropriately.

In order to reduce the size of this transfer file, the time steps, the spatial steps in the 3 directions, as well as the limits of the domain covered in the file, do not necessarily coincide with the respective values of the CFD analysis. Linear interpolations are used by FDS between its internal results to write the file, and linear interpolations are performed by SAFIR when reading the file to compute the relevant values at the requested positions in time and in space. Based on the data found in the transfer file, a series of 2D transient thermal analyses are performed along

207 the structural members and the results are stored in appropriate files. As these 2D temperature

208 distributions will be used subsequently to represent the temperature in beam finite elements, a

209 temperature distribution is calculated for each longitudinal point of integration of each beam

210 finite element; SAFIR uses 2 or 3 points of Gauss along the beam elements. In these 2D

211 thermal analyses, the impinging flux is computed for each boundary (in the sense of finite

212 element discretisation) of the section, depending on its orientation. As an approximation, the

213 position of the boundaries of the section in the fire compartment is the same for all boundaries

214 of a section (at the position of the node line of the beam finite element, based on the

215 assumption that half of the characteristic length of the section is small with respect to the size of

216 the compartment). For the boundaries on concave parts of the section, impinging radiative

217 intensities from certain direction are discarded if there is an obstruction by other parts of the

218 section. Mutual radiation between different boundaries of the section in the concave regions is

219 not considered. Generally, in the CFD model, the dimensions of a rectangular compartment

220 correspond to the clear distances between opposite walls. However, in the FE model, a slab is

221 generally modelled in correspondence to its centreline. Thus, the slab would fall outside the

222 CFD domain, and assumptions have to be made to determine thermal information at the slab

223 centreline.

224 ***4.2 Example***

225 *4.2.1 Configuration of the compartment*

226 In this example, a compartment similar to the one depicted in Fig. 2, i.e. a 51m x 9m x 4m

227 compartment with 20m x 3.25m opening size, is considered. While the compartment geometry

228 is similar to the one of configuration 1.b, there is a difference in the rate of heat release density.

229 Considering the maximum value of the rate of heat release curve of a cube and a floor averaged

230 distribution, the solid cribs are in this case spaced 2m away from each other to represent the

231 rate of heat release density of an office building, which is 250 kW/m^2 (EN1991-1-2, 2002). As for

232 previous configurations, the Fig. 7 depicts isolines representing the positions of the fire front in

233 the compartment, at different times. Though the initial spread of the fire is quite similar to that

234 seen for configuration 1.a, the subsequent progress is slower by about a factor of two until the

235 end of the fire, a trend which can be attributed to the greater spacing between the cribs, which

236 results in the fire taking significantly longer to spread between the individual fuel parcels, as well

237   as the reduction in the peak burning rate per unit floor area (i.e. 245 kW/m^2 versus 600 kW/m^2

238   for 1.a). Apart from the spread rate the behaviours otherwise appear to be broadly comparable.

239

240   *4.2.2 Steel structure*

241   To illustrate the capabilities of the CFD-FEM coupling, the steel framed structure made of hot

242   rolled steel profiles shown on Fig.8 is supposed to be present in the compartment described

243   above. In the FE analysis (in SAFIR, each column is discretized into 4 BEAM elements and

244   each beam of the frame is discretized into 6 BEAM elements. Two points of Gauss are defined

245   along the BEAM elements.. For the thermal analyses, the emissivity of steel was set to 0.7 and

246   the convection coefficient to 35 W/m²K, following EN 1991-1-2. The number of directions in

247   which the radiation intensities are computed is set to 72, which is recommended as minimum

248   when analysing structural members that entails shadow effects. For the subsequent mechanical

249   analysis, the frame located at mid-width of the compartment (spanning along X axis) is

250   considered. The steel sections of the beams are IPE 400 while those of the columns are HE 200

251   A, in steel grade S275. The columns are completely fixed at the base, while one direction has

252   been fixed at the top to avoid out of plane displacements. A uniformly distributed loading of 6,5

253   kN/m is applied on the beams, corresponding to 142 kg/m².

254

255   *4.2.3 Results*

256   Fig. 9.a shows one result of the thermal analysis performed by SAFIR: the isotherms after 41

257   minutes in the IPE400 beam in the middle of the first span (point A in Fig. 8). A clear difference

258   is observed between the lower flange and the upper flange, the latter being exposed to fire only

259   on 3 sides. A gradient can also be observed in the flanges from right (toward the centre of the

260   compartment) to left (toward the wall). Also, the lower part of the web is somehow protected by

261   the lower flange from the radiation intensities that come mainly from the bottom right direction

262   (i.e. the ground in the compartment). Fig. 9.b shows the evolution of the temperature in the

263   centre of the section in the central beam (from B to F) after 67 and 92 minutes. The offset

264   between the plots reflects the spread of the fire in the compartment. At 67 and 92 minutes, the

265   fire front is situated at X = 21 metres and X = 32 metres, with a fire thickness of approximately 6

266   meters and 8 meters, respectively. The steel temperature peaks are computed at X = 13 metres

267   and X = 24 metres, i.e. just after the fire passed. Fig. 10.a shows the node which is considered

268   for plotting the evaluation of the steel temperature along the column height (the central column

269   placed below point B in Fig. 8), which is shown in Fig. 10.b for three times: 90 minutes (when

270   the column is within in the fire zone), 100 minutes (when the fire zone starts to leave the

271   column) and 110 minutes This figure translates a thermal gradient along the height of the

272   compartment with maximum temperatures (steel temperatures are considered at the locations

273   of the Gauss Nodes in the column) and, as Fig. 9.b, reflects the spread of the fire in the

274   compartment.

275

276   The temperatures computed in the sections of the 3D beam finite elements that form the

277   structure are taken into account in a geometrically transient and materially nonlinear structural

278   analysis performed with SAFIR. Many different results can be obtained from this type of

279   analysis, such as the evolution of axial forces and bending moments in the elements, the

280   stresses in the elements, the displacements of the nodes and finally, the fire resistance time and

281   the failure mode (or the absence of failure). The evolution of the vertical displacement at the top

282   of the five columns from the central frame is represented on Fig. 11. As the structure does not

283   collapse, the vertical displacement is essentially elastic and is therefore a result of thermal

284   elongation. The travelling nature of the fire is highlighted by the time shift of the thermal

285   elongation in the columns B to F.

286

287   **5. Discussions and further improvements**

288   The sample cases presented illustrate the potential value of CFD for generating and analysing

289   fire dynamic conditions which influence the likelihood of fire spread. It is important to note that

290   these are numerical examples and not validation studies. Thus there are important provisos on

291   the interpretation of the results. Further work would be required to quantify any deviations

292   arising due to numerical effects.

293

294   Also, the methodology used for the representation of burning fuel has some limitations. Before a

295   cell reaches the ignition temperature, its heating is computed while considering heat exchanges

296   with the environment. But as soon as the ignition temperature is met, FDS represents the fire by

297　releasing volatile combustibles which, if all are burnt, results in the prescribed HRR curve. This

298　is done without considering the evolution of heat exchange with the environment. Moreover, the

299　uniform cubic shape of the obstruction prevents air flow through the object. Nevertheless, it was

300　concluded that this approach can yield a good representation of an isolated burning wood crib in

301　comparison with hand calculations of the upper and mean value of the mass loss rate (Degler J

302　and Eliasson A, 2015).

303

304　Furthermore, the details of glazing failure have been ignored at this stage, and more realistic

305　compartment geometries and boundary materials should also be considered. Crib burning rates

306　are affected by the proximity to the compartment boundaries but the simplified representation

307　adopted does not admit the known enhancement of the burning rate arising from the additional

308　heat transfer contribution in a corner fire.

309

310　Moreover, having demonstrated the value of the methodology, further systematic use of

311　numerical simulations will be undertaken to perform more comprehensive parametrical

312　analyses. The calibration of these simulations will also benefit from experimental tests from the

313　literature and those performed in the frame of the TRAFIR project. It will then be possible to

314　determine with more confidence the conditions in which a travelling fire may develop, or not,

315　and therefore inform on appropriate fire scenarios to be considered. Experimental campaign

316　launched in the frame of the same project and further CFD analyses are described in (Nadjai et

317　al. (2020); Charlier et al. (2020)).

318

319　Concerning SAFIR, parallelisation of the code which is currently under way, which will reduce

320　the CPU time requested for the large number of 2D thermal analyses performed in the sections.

321

322　**6. Conclusions**

323　Using the Fire Dynamics Simulator (FDS), different geometrical arrangements were modelled in

324　terms of compartment layout, opening size and ceiling height. A fire load composed of wood

325　cribs has been considered using discrete volumes arranged on regular grids, and a temperature

326　criterion on the volume surfaces was used to trigger the start of a predefined heat release curve.

327   Some useful quantitative measures of fire behaviour were extracted from the CFD results, in

328   particular the fire spread rates, facilitating analysis of characteristic behaviours. It was possible

329   to interpret all the observed trends in terms of fundamental principles of fire dynamics. The

330   method for study via this kind of representative simulations is built on several explicit

331   assumptions, but nevertheless permits a first assessment of the conditions required for fire

332   spread and provides an indication of some of the influential parameters and likely sensitivities.

333   In particular, for a given fire load and compartment dimensions, modifying the ventilation

334   conditions (i.e. the opening factor) showed a significant influence on the fire behaviour,

335   consistently with experimental observations (Gupta *et al*. 2020). In the present paper, the

336   studied configurations lead to travelling fire, without encountering ventilation controlled stages,

337   but other ventilation conditions (i.e. reduced openings) could obviously lead to such situations.

338   The implications of such design choices should therefore be investigated to assess the proper

339   fire scenarios to be considered.

340

341   Further, by considering the detailed results of the CFD analysis in a nonlinear

342   thermomechanical analysis of a structure located in the fire compartment, the coupling of the

343   structural response to the travelling fire characteristics has been demonstrated. In the presented

344   configurations, such methodology appeared adequate to properly translate the thermal effects

345   linked to the travelling nature of a fire on steel frames made of hot rolled profiles (as observed

346   through the thermal gradient within the sections and offset of the temperature versus time plots).

347

353

354   **References**

355 Charlier M, Vassart O, Dai X et al. (2020) A simplified representation of travelling fire

356 development in large compartment using CFD analyses. Accepted for the 11th Intl. Conf. on

357 Structures in Fire, 2020.

358

359 Dai X, Welch S and Usmani A (2017) A critical review of 'travelling fire' scenarios for

360 performance-based structural engineering. Fire Safety Journal 91: 568-578.

361

362 Dai X, Welch S, Rush D et al. (2019) Characterising natural fires in large compartments –

363 Revisiting an early travelling fire test (BST/FRS 1993) with CFD. Proceedings 15th International

364 Interflam Conference, London, UK.

365 Dai X, Welch S, Vassart O et al. (2020) An extended travelling fire method framework for

366 performance-based structural design. Fire and Materials 44: 437–457.

367

368 Degler J and Eliasson A (2015) A Priori Modeling of the Tisova Fire Test in FDS, Bachelor's

369 Thesis, Luleå University of Technology, SE.

370

371 Degler J, Eliasson A, Anderson A et al. (2015) A-priori modelling of the Tisova fire test as input

372 to the experimental work. Proceedings 1rst International Conference on Struct. Safety under

373 Fire & Blast, Glasgow, UK.

374

375 EN1991-1-2 (2002). Eurocode 1: Actions on structures - Part 1-2: General actions-Actions on

376 structures exposed to fire. CEN, Brussels.

377

378 Franssen JM and Gernay T (2017) Modeling structures in fire with SAFIR®: theoretical

379 background and capabilities. Journal of Structural Fire Engineering 8: 300-323.

380

381 Gupta V, Hidalgo JP, Cowlard A, et al. (2020) Ventilation effects on the thermal characteristics

382 of fire spread modes in open-plan compartment fires. Fire Safety Science 13 (in press)

383

384   Hidalgo JP, Cowlard A, Abecassis-Empis C et al. (2017) An experimental study of full-scale

385   open floor plan enclosure fires. Fire Safety Journal 89: 22-40.

386

387   Horová K (2015) Modelling of Fire Spread in Structural Fire Engineering. PhD thesis, Czech

388   Technical University in Prague.

389

390   Horová K, Jána T and Wald F (2013) Temperature heterogeneity during travelling fire on

391   experimental building. Advances in Engineering Software 62-63: 119-130.

392

393   McGrattan K, Hostikka S, McDermott R et al. (2017) Fire Dynamics Simulator User's Guide,

394   Sixth Edit. National Institute of Standards and Technology (NIST).

395

396   Nadjai A, Alam N, Charlier M et al. (2020) Travelling fire in full scale experimental building

397   subjected to different ventilation conditions. Accepted for the 11th Intl. Conf. on Structures in

398   Fire, 2020.

399

400   Rush D, Lange D, Maclean J et al. (2015) Effects of a Travelling Fire on a Concrete Column -

401   Tisova Fire Test. Proceedings of the 2015 ASFE Conference.

402

403   Society of Fire Protection Engineers Handbook (2002) Fire Protection Engineering, Third

404   Edition, National Fire Protection Association, USA.

405

406   Stern-Gottfried J and Rein G (2012) Travelling fires for structural design - Part I: Literature

407   review. Fire Safety Journal 54: 74-85.

408

409   Thomas I, Moinuddin K, Bennetts I (2005) Fire development in deep enclosure. Fire Safety

410   Science 8: 1277-1288.

411

412   Tondini, N., Vassart, O. Franssen, J.-M. (2012) Development of an interface between CFD and

413   FE software. Proceedings of the 7th International Conference on Structures in Fire M. Fontana,

414   A. Frangi, M. Knobloch, Switzerland.

415

416   Tondini N, Morbioli A, Vassart O et al. (2016) An integrated modelling strategy between a CFD

417   and an FE software: Methodology and application to compartment fires. Journal of Structural

418   Fire Engineering 7 Issue 3: 217-233.

419

420   Welch S, Miles S, Kumar S et al. (2008) FIRESTRUC – Integrating advanced three-dimensional

421   modelling methodologies for predicting thermo-mechanical behaviour of steel and composite

422   structures subjected to natural fires. Fire Safety Science 9: 1315-1326.

423

424

425   **Figure captions (images as individual files separate to your MS Word text file).**
426   Figure 1. Heat release rate of one burning cube
427   Figure 2. Model of configuration 1.b
428   Figure 3. Fire spread time vs. compartment location, under configuration 1.a
429   Figure 4. Fire spread time vs. compartment location, under configuration 1.b
430   Figure 5. Fire spread rate vs. compartment location, under configurations 1.a and 1.b
431   Figure 6. Fire spread time vs. compartment location under a) configuration 2.a; b) configuration
432   2.b
433   Figure 7. Fire spread time vs. compartment location, under configuration to illustrate the
434   capabilities of the CFD-FEM coupling
435   Figure 8. Steel structure in the compartment and solid cribs
436   Figure 9. Steel temperatures in beams. a) Isotherms after 41 minutes at A; b) Evolution along
437   central beam B-F
438   Figure 10. a) Location of the node considered for b) the evaluation of the steel temperature
439   along the height of the central column
440   Figure 11. Evolution of the elongation of the columns in the central frame as a function of time
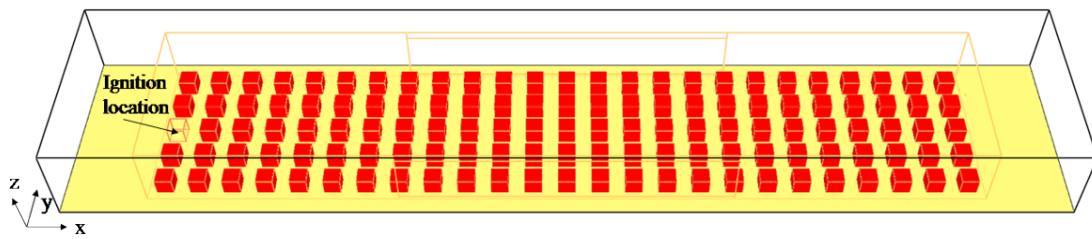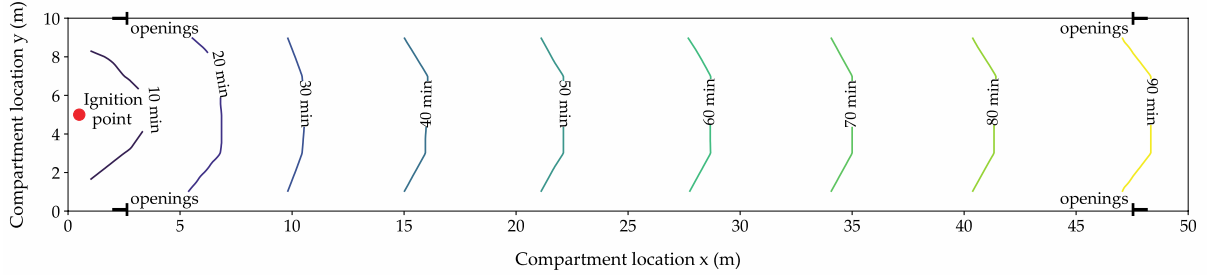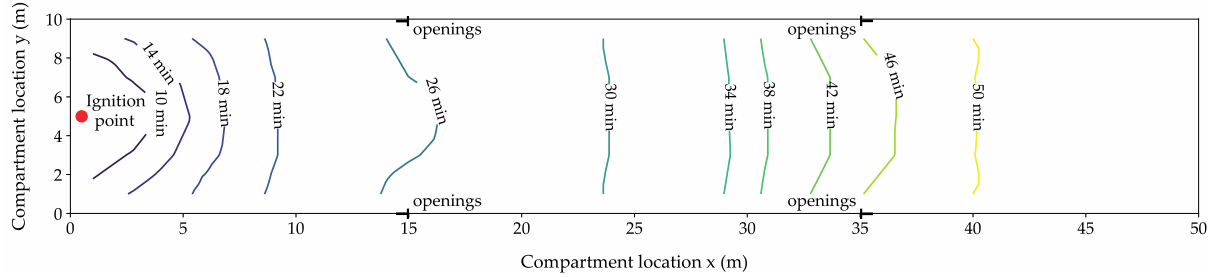441

442   Fig. 1
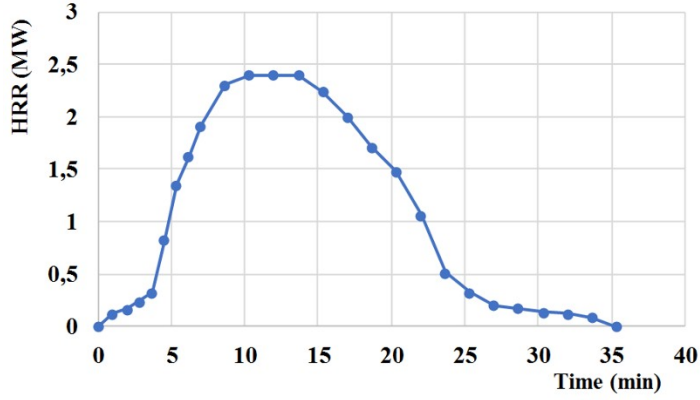
443
444
445   Fig. 2

446
447
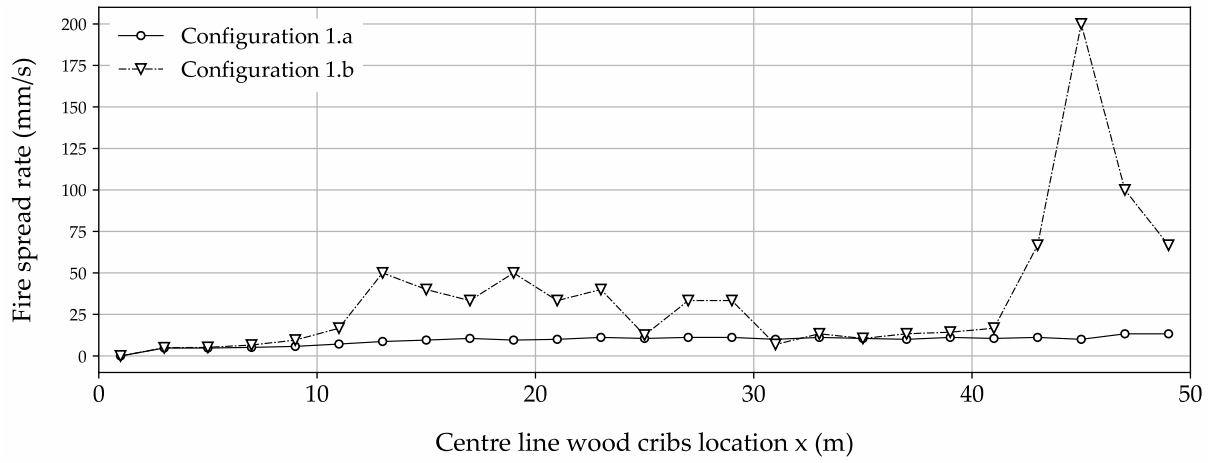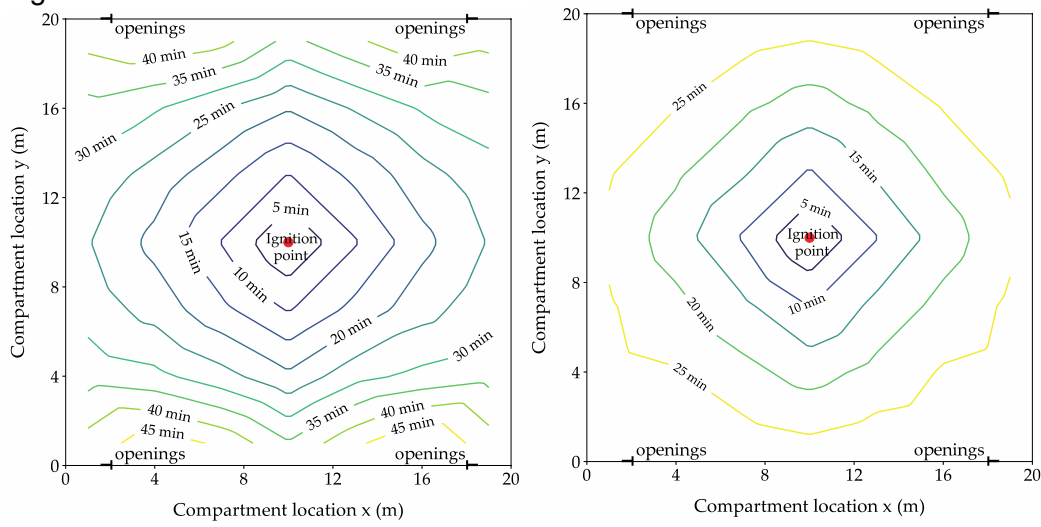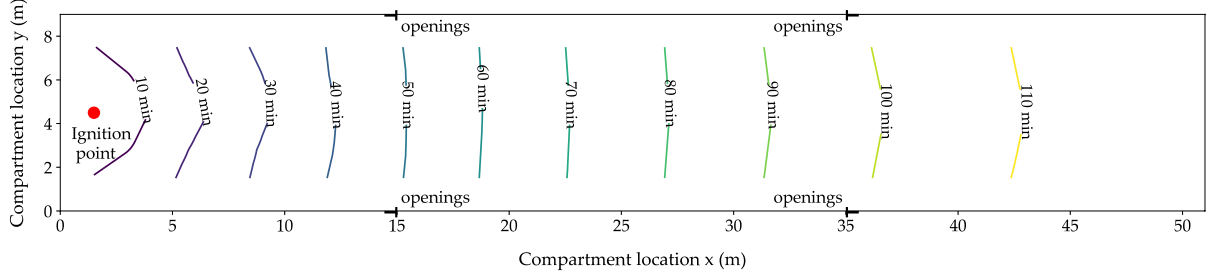448   Fig. 3

449
450   Fig. 4

451
452
453
454
455   Fig. 5

456
457
458   Fig. 6
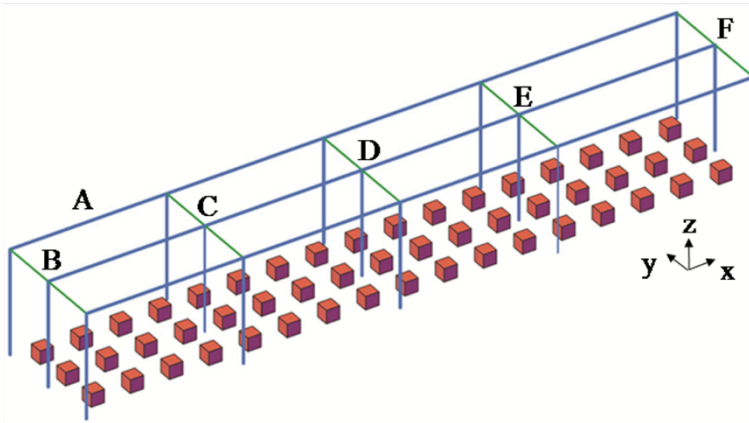

459
460
461
462   Fig. 7

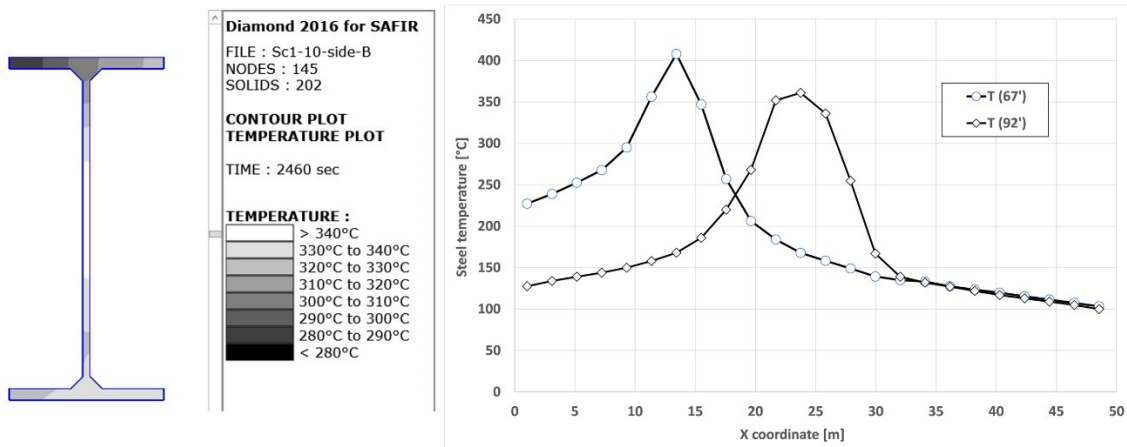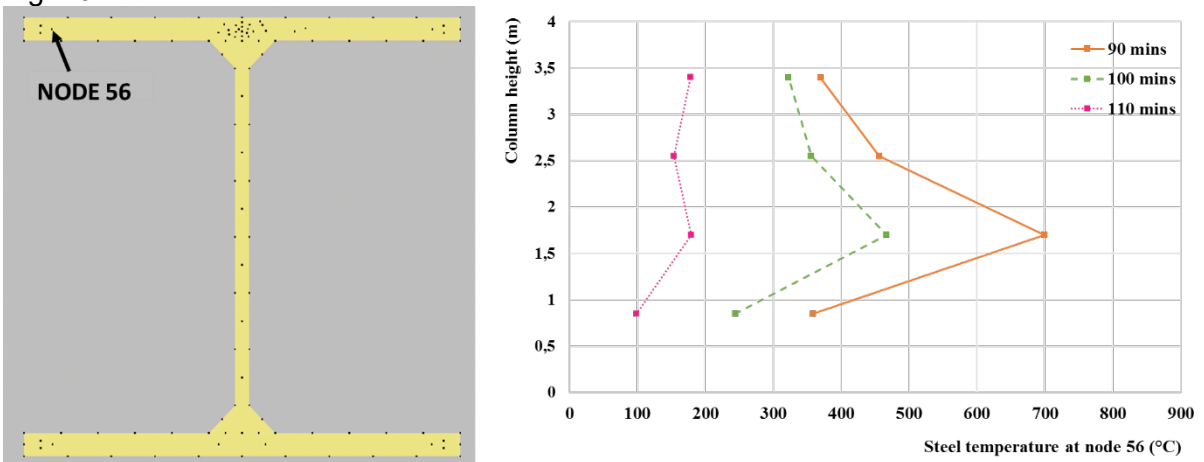

463
464
465
466
467
468   Fig. 8

469

470

471   Fig. 9

472

473

474   Fig. 10

475

476

477

478   Fig. 11

479
480
481